Nanoscale

Structural and Electrical Characterizations of Monolithic Core-Double Shell n-GaN/Al/p-AlGaN Nanowire Heterostructures Grown by Molecular Beam Epitaxy

Journal:	*Nanoscale*
Manuscript ID	NR-ART-01-2019-000081.R1
Article Type:	Paper
Date Submitted by the Author:	22-Jan-2019
Complete List of Authors:	Sadaf, Sharif; National Research Council Canada; McGill University, Electrical and Computer Engineering Ra, Yong-Ho; McGill University Zhao, Songrui; McGill University Szkopek, Thomas; McGill University Mi, Zetian; University of Michigan

SCHOLARONE™
Manuscripts

Structural and Electrical Characterizations of Monolithic Core-Double Shell *n*-GaN/Al/*p*-AlGaN Nanowire Heterostructures Grown by Molecular Beam Epitaxy

S. M. Sadaf[1,2], Y.-H. Ra[2], S. Zhao[2], T. Szkopek[2], and Z. Mi[2,3]

[1]*Advanced Electronics and Photonics, National Research Council Canada, Ottawa* K1A 0R6*,*

[2]*Department of Electrical and Computer Engineering, McGill University, 3480 University Street, Montreal, Quebec H3A 0E9, Canada*

[3]*Department of Electrical Engineering and Computer Science, Center for Photonics and Multiscale Nanomaterials, University of Michigan, Ann Arbor, Michigan 48109, USA*

[*]*E-mail: sharif.sadaf@nrc-cnrc.gc.ca; ztmi@umich.edu*

We have studied the epitaxy and structural characterization of monolithic *n*-GaN/Al/*p*-AlGaN nanowire heterostructure. It is found that, high quality, nearly defect free, full shell epitaxial Al can be grown *in situ* on Al(Ga)N nanowires and vice-versa. Detailed scanning transmission electron microscopy (STEM), high-resolution transmission electron microscopy (HRTEM) and X-ray diffraction (XRD) characterizations suggest that Al (111) plane maintains an epitaxial relationship with Al(Ga)N (0001) in the nanowire growth direction. Full ultraviolet composition range (340 nm-210 nm) Al/Al(Ga)N core-double shell nanowire backward diode characteristics were investigated. We have demonstrated a monolithic n^{++}-GaN/Al/p^{++}-Al(Ga)N nanowire backward diode, wherein an epitaxial Al layer serves as the tunnel junction. Such an Al(Ga)N-based *n-p-n* nanowire backward diode exhibits record low resistivity ($<1.5\times10^{-4}$ $\Omega.cm^2$) and low turn-on voltage of ~2.7 V

Epitaxy of dissimilar materials (distinctly different properties, crystal structures and lattice parameters) commonly known as 'heteroepitaxy' promises to introduce different novel functionalities.[1] Among the heteroepitaxial interfaces, metal/semiconductor epitaxy holds tremendous promise for numerous electronic/optoelectronic applications.[2] Previously, various epitaxial metals/GaAs interfaces, including Al/GaAs, Ag/GaAs, Fe/GaAs, Au/GaAs, Co/GaAs have been extensively studied by molecular beam epitaxy (MBE) to realize improved device performance[1, 3-5]These extensive epitaxial metal/GaAs-based studies are primarily due to the importance of prototype III-V semiconductor GaAs and well known GaAs-based device applications. In addition, the lattice mismatch between the common Al metal and GaAs is relatively small (~1.4%), and they have similar crystal structures.[6] On the other hand, III-nitride semiconductors are considered ideal for a broad range of electronic and optoelectronic device applications. It is well established that Al is critically important metal for a wide range of electronic/optoelectronic devices due to CMOS compatibility, ohmic contact formation with different semiconductors, and superconducting bahaviour.[7] To date, however, it has remained challenging to realize high quality epitaxy between metal and Al(Ga)N due to the prohibitively large lattice mismatch[2, 8] Therefore, there have been very few studies on the epitaxy of metal/Al(Ga)N semiconductors, and these reports have been restricted to metal/Al(Ga)N planar structures.[8] In general, the performance of large lattice mismatched (~10% or more) epitaxial metal/semiconductors planar structures has been limited due to the presence of large densities of defects/dislocations.[2, 3, 9] Still, a few reports demonstrated that different metals ranging from Ni, Pd, Pt, Al, Ti, Hf, Fe and Mg can be grown epitaxially on GaN in both ultra-high vacuum and in conventional vacuum conditions with limited success.[2, 3, 8-14] It was also reported that various metal/GaN and/or metal/GaAs epitaxy is possible even with the presence of a thin native oxide on

GaN or GaAs.[8] Previous reports suggest that GaN/metal/GaN sandwich structure can be realized in planar geometry without any noticeable intermixing. Even so, the interlayer metal suffers from two-dimensional tensile stress due to large lattice and thermal co-efficient mismatch.[15]

Compared to conventional planar structures, III-nitride nanowires exhibit significantly reduced defects and dislocations due to the effective lateral stress relaxation. In addition, because of the reduced dopant formation energy in nanowire structures, significantly improved dopant ionization can be realized.[16, 17] Given these advantages, III-nitride nanowires are considered promising in light-emitting diodes, lasers, and power electronics.[16] Recent reports suggest that Al(Ga)N nanowires can be epitaxially grown on different metals and graphene.[18, 19] Moreover, nearly defect-free, atomically clean monolithic metal/Al(Ga)N interface in nanowire heterostructures can be potentially employed to realize low resistance backward diode.[12, 20, 21]

Until recently, a comprehensive study of the epitaxial growth and characterization of Al/Al(Ga)N structures has remained elusive due to several challenges. First, Al is a face centered cubic (fcc) metal with relatively low melting point (~660ºC) that limits Al growth/deposition temperature both *in situ* or *ex situ*.[1] Second, direct epitaxial fcc Al metal growth on wurtzite GaN critically depends on the growth temperature, growth rate, ultrahigh vacuum condition, and the surface quality of the GaN layer.[8] Third, the close packed Al (111) plane has a significantly large lattice-mismatch (~10.2%) with the close packed GaN basal plane (0001) that induces tensile strain in the Al layer.[8] However, it was reported that an epitaxial Al layer can be formed on GaN at different temperatures, the Al film quality largely depends on the Al layer thickness and high quality epitaxy was observed beyond a critical thickness.[8] Conversely, it was also reported that high quality GaN can be grown on various metal layers at different growth temperatures using MBE.

Low resistance, efficient tunnel junctions or backward diodes integrated with photonic devices offer several potential benefits. First, tunnel junctions enable the replacement of highly resistive *p*-GaN contacts with *n*-GaN that significantly reduces optical absorption loss, gives improved current spreading and significantly reduced contact resistance.[12, 16] Second, tunnel junctions can act as a carrier type conversion center thereby enabling efficient *non-equilibrium* hole injection that significantly improves radiative efficiency in the LED/laser active region.[12, 16, 20, 22, 23] Third, cascaded *p*-*n* junctions/ LEDs can be serially connected by low resistance tunnel junctions, and the so called "efficiency droop" problem can be significantly circumvented by cascaded LEDs.[16, 24, 25] Yet, the demonstration of efficient, low resistance stand-alone tunnel junctions (backward diodes) using large bandgap AlGaN nanowires or thin films remains very challenging. To date, however, the resistance and the overall performance of III-nitride tunnel junctions has been severely limited by the *p*-type dopant solubility limit, prohibitively large dopant ionization energy (200-600 meV) and wide band gaps (3.4 eV to 6.2 eV).[26]

In this context, we have performed a detailed investigation of the MBE growth of Al metal on wide band gap *n*-GaN nanowire as well as *p*-AlGaN nanowire on Al. We have extensively studied the epitaxy and other morphological/structural characterizations of Al/Al(Ga)N nanowire by transmission electron microscopy (TEM), scanning electron microscopy (SEM) and X-ray diffraction (XRD). Our detailed studies suggest that high quality, nearly defect-free Al metal can be epitaxially grown on Al(Ga)N with Al thickness ranging from ~1.6 nm to ~15 nm in the c-axis growth direction without any noticeable misfit dislocations. It is also observed that sufficiently thick Al(Ga)N can be epitaxially grown on Al metal as well. Such high-quality *n*-GaN/Al and Al/*p*-Al(Ga)N interface suggests that dislocation/stacking-fault free interface can be possibly realized in *n*-GaN/Al/*p*-Al(Ga)N nanowire heterostructure due to the effective stress relaxation in

the sidewalls. Subsequently, we have also demonstrated record low-resistance n^{++}-GaN/Al/p^{+}-$Al_{0.15}Ga_{0.85}N$ nanowire backward diodes.

In this work, we have studied three different types of epitaxial *n*-GaN/Al/*p*-AlGaN nanowire structures. These nanowire structures were grown under similar growth conditions except the Al growth duration was varied to examine the dependence of metal/semiconductor epitaxy on the Al layer thickness. The studied structures are illustrated in Fig. 1a, which are denoted as epitaxial nanostructure A, nanostructure B and nanostructure C. The nanostructure A consists of 340 nm *n*-GaN, 25 nm n^{++}-GaN, 1.6 nm Al, 25 nm p^{++}-$Al_{0.15}Ga_{0.85}N$, and 30 nm *p*-$Al_{0.15}Ga_{0.85}N$ capping layer. Nanostructures B and C consist of a similar structure except that the thicknesses of Al were increased to ~5 nm and ~16 nm, respectively. The growth rate of the GaN segment is calculated to be 300 nm/hour, whereas the growth rate of the AlGaN segment is 100 nm/hour. Illustrated in Fig. 1b is the scanning electron microscopy (SEM) image of Al nanostructure A taken with 45º angle. As can be seen, the nanowires are vertically aligned on the Si substrate and exhibit relatively uniform height and size distribution.

All the epitaxial metal/semiconductor nanostructures were grown by plasma-assisted MBE on *n*-Si (111) substrates under nitrogen rich condition without using any external metal catalyst. Prior to loading the Si substrate into the MBE growth chamber, the thin native oxide was removed with hydrofluoric acid (10%), and further *in situ* desorbed at ~770ºC. The N_2 flow rate and forward plasma power were kept at 1.0 standard cubic centimeter per minute (sccm) and ~350 W during the growth. Importantly, MBE provides unique opportunity to realize *in situ* Al/III-nitride epitaxy since it has an elemental Al source, and this eliminates the need of *ex situ* Al deposition and GaN surface cleaning. The substrate temperature was kept at ~780ºC for the growth of *n*-GaN. For the heavily doped n^{++}-GaN region, the growth temperature was lowered to 640ºC. The epitaxial Al

layers was grown at ~460º C and subsequently capped with a thin layer of Ga. To avoid the formation of AlN or Al-rich AlGaN, the nitrogen plasma was turned off during the Al layer growth. It was previously reported that after a few monolayer (ML) growth (1 ML= 0.234 nm, planar distance between Al (111) planes), the crystalline quality of the epitaxial Al-layer improves and consistently shows similar epitaxial Al layers up to ~40 nm.[8] Therefore, it is expected that high quality, nearly defect-free epitaxial Al-layers can be grown with different thicknesses. The substrate temperature was then increased to ~630ºC (below Al melting point) for the growth of *p*-AlGaN and subsequently capped with another layer of *p*-$Al_{0.15}Ga_{0.85}N$. The top *p*-$Al_{0.15}Ga_{0.85}N$ grown at low temperature is believed to seal the undergrown metallic Al. Doping concentration and degeneracy in the epitaxial nanostructures were controlled by the Si (*n*-doping) and Mg (*p*-doping) effusion cell temperatures. Si and Mg doping concentrations in the heavily doped *n*-GaN and *p*-AlGaN segments of the nanostructure were in the ranges of 5×10^{19} and 1×10^{20} cm^{-3}, respectively. In this growth process, the Al and Ga beam equivalent pressures of 2.5×10^{-8} and 5×10^{-8} Torr, respectively, were maintained.

Structural properties of the different epitaxial Al/AlGaN nanowire heterostructures were subsequently investigated by scanning transmission electron microscopy (STEM) and high-resolution transmission electron microscopy (HR-TEM) using a JEOL JEM-2100F equipped with a field emission gun operated at 200 kV. The sample was prepared by dispersing Al/AlGaN nanowires on a Cu grid, and high angle annular dark field (HAADF) STEM imaging was used with an electron beam diameter of approximately 0.2 to 0.7 nm. Shown in Fig. 1c, the interfaces between the epitaxial Al layer and subsequent *p*-AlGaN layer and between the Al layer and bottom *n*-GaN were characterized by HR-TEM. The detailed HR-TEM analysis further confirmed there were no noticeable stacking faults, biaxial strain induced threading dislocations or intermixing at

any of the interfaces, which is in direct contrast to planar Al/GaN interface. From the lattice fringe image as shown in Fig. 1c, it is seen that the interplanar spacing is 0.233 nm in Al layer, which corresponds to that of Al (111) plane. The interplanar distance (lattice fringes) in *n*-GaN and *p*-Al(Ga)N are derived to be 0.254 nm and 0.250 nm, respectively. Such interplanar spacings of GaN and Al(Ga)N are consistent with the ideal unstrained condition.[17, 27, 28] It is worthwhile mentioning that the lattice constant of Al (111) is 0.289 nm, whereas the lattice constant of GaN (0002) plane is 0.319 nm. As such, the lattice-mismatch between the epitaxial Al (111) and Ga (0002) is ~10%. Such large lattice mismatch induced dislocations can be relaxed in the nanowire sidewalls, and dislocations/stacking faults free interfaces can be realized. We have also confirmed this heteroepitaxy by X-ray diffraction (XRD) (to be discussed in the later section). Illustrated in Fig. 2a are the STEM images of Al/AlGaN nanowire structure (thick Al-layer), wherein the different segments are identified. In high-magnification STEM images shown in Fig. 2b, the Al layer is clearly observed with ~16 nm thickness. Shown in Fig. 2a and 2b, the Al/AlGaN nanowire heterostructure consists of double shell and GaN core. It is seen that, the inner shell is purely metallic, whereas the outermost one is AlGaN shell. Energy dispersive X-ray spectroscopy (EDXS) analysis was further performed to study the compositional variations of the epitaxial *n*-GaN/Al/*p*-$Al_{0.15}Ga_{0.85}N$ nanostructure. To further understand the compositional variations, we have studied both thick and thin Al/AlGaN nanostructures by EDXS point analysis. Supplementary Fig. S1 illustrates the STEM image and EDXS analyses of different segments of thin Al/AlGaN nanostructures. An EDXS point analysis was done in the vicinity of the Al-layer, shown in Fig. 2c, which provided clear evidence for the presence of Al. The GaN nanowire with Al layer is surrounded by another AlGaN shell which was formed during the epitaxy of subsequent p^{++}-$Al_{0.15}Ga_{0.85}N$ segment and *p*- $Al_{0.15}Ga_{0.85}N$ capping layer. It can also be seen that a thin layer of Al

shell forms in the sidewalls (*m*-planes of GaN core). EDXS point analysis was carried out in the p^{++}-$Al_{0.15}Ga_{0.85}N$ layer, Al layer (in the sidewalls) and *n*-GaN layer. As can be seen in Fig. 2c, point analysis in the *n*-GaN region also gives sensitivity to Al which is higher than the Al-signal in the *p*-$Al_{0.15}Ga_{0.85}N$ region. Since the *n*-GaN region is surrounded by inner Al metal shell and outer *p*-$Al_{0.15}Ga_{0.85}N$ shell, the electron beam directed perpendicular toward the *n*-GaN region gives collective sensitivity to Al which sums up to be greater than the Al-signal in the *p*-$Al_{0.15}Ga_{0.85}N$ region. In consequence, even though the beam was directed toward the Al-layer, Ga and Cu signals were also detected from the surrounding AlGaN outer shell structure and Cu grid due to the transmitted beam. We have performed EDXS line profile analysis along the lateral dimension of the different sections of the nanowire (lines A, B, C). These lateral EDXS line scan (line scan B) unambiguously confirms the presence of double shell (Al inner shell and AlGaN outer shell). We have also performed line scans along the length of the nanowire (n^{++}-GaN to p^{++}-$Al_{0.15}Ga_{0.85}N$ through the Al layer). As can be seen in Fig. 3, line scan A confirms the presence of Al layer, whereas line scan B shows Ga rich *n*-GaN in the center. Line scan C confirms the presence of low Al% *p*-AlGaN layer. It is worthwhile mentioning that due to the presence of very thin ~1.5 nm-2.5 nm Al layer (in thin Al layer, nanostructure A), similar line scans along the nanowire do not give greater sensitivity or signal for the presence of Al. Our detailed TEM study suggests that point analysis at different segments of the nanowires can reliably identify AlGaN segments and/or Al layer/shell. Conversely, EDXS line analyses along the lateral dimension are best suited for identifying the Al metal shell and/or AlGaN shell region, and along the nanowire direction through the Al layer confirms the presence of Al.

To further anlyze the epitaxial relationship between Al metal and Al(Ga)N nanowires, the spontaneously grown large area nanowire samples were characterized by XRD. The XRD

experiments were carried out with Cu Kα radiation using a Panalytical X-pert Pro MRD system equipped with a Ge (220) hybrid monochromator. Fig. 4 shows the θ/2θ scan performed to determine the out of plane orientation of Al/Al(Ga)N nanowires (nanostructure C). Apart from mthe peaks form Si substrates, peaks from GaN (0002) and Al (111) are also seen. The strong sharp peak at 2θ=34.6º along with another relatively weak broad peak at 2θ=38.4º correspond to the reflection from wurtzite GaN (0002) and fcc Al (111). The presence of Al (111) and GaN (0002) peaks suggest that fcc Al (111) plane maintains an epitaxial relationship with GaN (0002) basal plane in the growth direction. It is worthwhile mentioning that the diffraction peak corresponds to Al (111) plane shifts toward higher angle is likely due to the tensile stress caused by the thermal expansion co-efficient mismatch.[9]There could be a critical thickness limit for Al due to large lattice or thermal co-efficient mismatch.

We have subsequently studied four different types of Al(Ga)N backward diodes exploiting metal/semiconductor epitaxial interface, including n^{++}-GaN/Al/p^{++}-$Al_{0.15}Ga_{0.85}N$, n^{++}-GaN/Al/ p^{+}-$Al_{0.50}Ga_{0.50}N$, n^{+}-$Al_{0.50}Ga_{0.50}N$/Al/p^{+}-$Al_{0.50}Ga_{0.50}N$, and n^{+-}AlN/Al/p^{+}-AlN, illustrated in Supporting Fig. S2, which are denoted as Diode A, B, C and D. Ga and Al beam equivalent pressures (BEPs) of ~2-3.5×10^{-8} and 1-2×10^{-8} Torr were kept, however, the substrate temperature was varied to tune the Al composition. Here, we have studied all the backward diode structures in *n*-*p*-*n* configuration, where heavily doped n^{++}-Al(Ga)N/Al/p^{+}-Al(Ga)N backward diode is serially connected to a GaN-based *p*-*n* junction. It is worthwhile mentioning that such *n*-*p*-*n* backward diode is not limited by high *p*-contact resistance, and therefore, it is envisioned that the intrinsic carrier transport of the backward diode can be better comprehended. It was also demonstrated that heavily Mg-doped *p*-GaN up nanowire structures generally exhibit relatively poor crystalline quality including non-uniform nanowire density, height, and rough surface morphology.[29, 30]

Therefore, subsequent device processing becomes difficult due to contact planarization and metallization issues. During the TJ device fabrication process, the nanowire arrays were first planarized using a polyimide resist layer, followed by O_2 plasma etching to expose the nanowire top surface. Ti (40 nm)/Au (200 nm) and Ti (20 nm)/Au (100 nm) metal layers were then deposited on the nanowire surface and the backside of the Si substrates to serve as *n*-metal contacts, respectively. The fabricated devices with metal contacts were annealed at ~500 ^{o}C for 5 mins in nitrogen ambient.

Current-voltage characteristics of all the backward diode nanowire structures (Diode A, B, C and D) were measured under continuous wave (CW) biasing conditions at room temperature. During the measurement, a negative bias was applied on the top surface for *n*-GaN (since all the structures are in *n*-*p*-*n* configuration). As such, the *p*-*n* junction was forward biased (a resistor) and the serially connected backward diode was reversely biased. Shown in Fig. 5a , all the devices exhibit clearly rectifying backward diode characteristics. The measured device areal size is 500×500 μm^2, and the nanowire filling factor is in the range of ~30%-50%. Shown in Fig. 5a, the *n*-*p*-*n* backward diode device (Diode A) shows a sharp turn-on voltage of ~2.7 V. The device total specific resistivity estimated from the linear region of the forward I-V characteristics is ~$9\times10^{-4}\ \Omega\ .cm^2$ or less, for the backward diode nanowire device (Diode A). This specific device resistivity for different devices includes *p*- and *n*-contact resistance, resistance of *p*-/*n*- junction and resistance of backward diode itself. Taking these factors into account, the upper limit of n^{++}-GaN/Al/p^{++}-$Al_{0.15}Ga_{0.85}N$ backward diode resistance (Diode A) is estimated to be ~$1.5\times10^{-4}\ \Omega\cdot cm^2$, or less (shown in the Supporting Fig. S3). In addition, the device showed only ~3V forward voltage drop at 100 A/cm^2. Such excellent device properties are attributed to the efficient *p*-type doping, nearly defect-free growth, reduced barrier height at Al/p^{++}-Al(Ga)N interface, excellent current transport

through the epitaxial Al metal layer, and the elimination of resistive *p*-(Al)GaN contact. As shown in Fig. 5a, the total specific resistivity for Diode B is ~1×10^{-3} Ω.cm^2, and therefore, the upper limit of n^{++}-GaN/Al/p^{++}-$Al_{0.50}Ga_{0.50}N$ is ~9×10^{-4} Ω.cm^2. This result suggests that efficient inter-band conduction critically depends on the barrier height (ϕ_b) and depletion region width (w) at Al/p^{++}-Al(Ga)N interface. Furthermore, different turn-on voltages in the devices are also attributed to the increased barrier height/depletion width at p^{+}-Al(Ga)N/Al interfaces and therefore, increased voltage drop was recorded for Diode B, C and D. Shown in the inset of Fig. 5a, For Diode C and Diode D, the turn-on voltage and specific resistivity is significantly increased with the increase of Al mole fraction and addition of *n*-AlGaN layer at the bottom interface. It confirms that inter-band tunneling not only depends on the Al/p^{++}-Al(Ga)N interface and Al mole fraction, but also depends on the n^{++}-AlGaN/Al interface. This also suggests that efficient ohmic/quasi-ohmic contact formation at the interfaces is critical for monolithic metal/wide bandgap AlGaN nanowire tunnel junction. It is worth pointing out that the carrier transport can be affected by the presence of metallic (Al) inner shell and semiconducting (*p*-AlGaN) outer shell. There could be parasitic leakage current through the Al shell layer, howeever, by the presence of outer *p*-AlGaN passivating shell layer the leakage current can be further compensated. Therefore, the total reverse leakage current should be negligible. It is envisioned that with further optimization of the doping and epitaxy process, both the turn-on voltage and resistivity of Al/Al(Ga)N backward diodes can be further reduced.

The schematic band diagrams of different Al/Al(Ga)N backward diodes are shown in Fig. 5. As can be seen in Figs. 5b and 5c, Al metal (work function 4.08 eV) can readily form an ohmic tunnel contact to heavily doped n^{++}-Al(Ga)N. On the other hand, with heavy Mg-doping, the depletion width at Al/$Al_{0.15}Ga_{0.85}N$ interface is decreased. It is worthwhile mentioning that the carrier

tunneling probability critically depends on the depletion region width (w) at metal/p^{++}-Al(Ga)N interface. The depletion region width (w) can be calculated by $\sqrt{\frac{2\varepsilon_s\phi_b}{q\,N_A}}$, where $\boldsymbol{\varepsilon}_s$ is the dilectric constant ($9.8\boldsymbol{\varepsilon}_o$), ϕ_b is the barrier height between metal/p-Al(Ga)N, q is the hole charge and N_A is the Mg-doping concentration. The calculated depletion region widths at Al/ p^{++}-$Al_{0.15}Ga_{0.85}N$ and p^{+}-$Al_{0.50}Ga_{0.50}N$ are calculated to be ~2.5 nm and ~34 nm, respectively. As such, carrier can efficiently tunnel from the filled valence band of p^{++}-Al(Ga)N through the epitaxial Al metal layer due to the reduced depletion width (shown in Fig. 5b). This transport mechanism is similar to field emission (FE) when the p-type Al(Ga)N is heavily doped (N_A >2×10^{19} cm^{-3}).[31] In addition, due to the presence of deep level defect (DLD) bands in p^{+}-Al(Ga)N and interfacial traps, carrier tunneling from p^{++}-Al(Ga)N to Al is significantly enhanced in a manner similar to trap-assisted tunneling (TAT).[12, 31, 32] Due to the moderate p-type doping (N_A ~1×10^{18} cm^{-3}) in $Al_{0.50}Ga_{0.50}N$, the depletion region width (w=34 nm at Al/p^{+}- $Al_{0.50}Ga_{0.50}N$ interface) and barrier height (ϕ_b= 1.05 eV at Al/p^{+}- $Al_{0.50}Ga_{0.50}N$ interface) are increased resulting in limited carrier tunneling. It is suggested that thermionic emission (TE) is dominant due to such large band gaps and related high potential barrier (Fig. 5c).[30, 31] For n^{+}-AlGaN/Al/ p^{+}-AlGaN and n^{+}-AlN/Al/ p^{+}-AlN the depletion width and barrier height are further increased (at both interfaces) due to the larger ionization energies, for both Mg and Si, and large band gaps with increasing Al concentration.

Fig. 5d shows the temperature-dependent I-V curves for the backward diode A (measured device areal size is 500×500 μm^2). An important figure of merit for backward diode is the curvature co-efficient at zero voltage defined as $\gamma=\frac{\frac{\delta^2 I}{\delta V^2}}{\frac{\delta I}{\delta V}}$. The measured γ is 14 V^{-1} at 300 K for Diode A, which is insensitive to temperature as γ remains constant even at low temperature (γ= 15 V^{-1} at 77 K). It is worthwhile mentioning that such a constant figure of merit, γ is lower than the room temperature

thermionic limit, $^{q}/_{kT}$~ 40 V^{-1} (generally associated with Schottky barrier), suggests that carrier transport is not limited by Schottky barrier at either interface. Such a low γ value further suggests that excellent dopant incorporation in *n*- and *p*-sides that govern ohmic/quasi-ohmic carrier transport through the Al-tunnel junction. Note that γ=14 V^{-1} measured in this study is in good agreement with the previously reported large band gap backward diodes.[33, 34]

In summary, we have investigated the MBE growth of *n*-GaN/Al/*p*-AlGaN nanowire heterostructures. Our detailed studies suggest that, nearly dislocation-free GaN/Al/Al(Ga)N nanowires can be grown epitaxially on Si substrate. We have also characterized and analyzed the epitaxial Al-layer quality by STEM, HR-TEM and XRD. It is found that epitaxial Al layers with different thicknesses can be grown on Al(Ga)N nanowires. This study suggests that the monolithic Al/Al(Ga)N nanowire epitaxy would enable different novel functionalities and improve III-nitride based optoelectronic/electronic devices. The low-resistance backward diode integrated with a *p*-*n* junction eliminates the need of polarization engineering. Our comprehensive study also suggests that specific resistivity critically depends on the Al molar fraction, *p*-/*n*-doping and related depletion width. The lowest specific resistivity ~1.5×10^{-4} Ω·cm^2 was measured with a turn-on voltage ~2.7 V. Such a new class of AlGaN-based nanowire backward diode offers a unique approach for achieving ultra-high efficiency III-nitride electronic devices. It is envisioned that the metal/semiconductor nanowire epitaxy can be further improved by utilizing selective area epitaxy wherein Al or other metals can be grown epitaxially on different semi-polar or non-polar Al(Ga)N nanowire facets.[35]

ACKNOWLEDGEMENTS

This work was supported by the Natural Sciences and Engineering Research Council of Canada (NSERC) and U.S. Army Research Office under the Grant No. W911NF-15-1-0168. Part of the work was performed in the Micro-fabrication Facility at McGill University. Electron microscopy images and analysis were carried out at the Facility for Electron Microscopy Research (FEMR), McGill University and at Ecole Polytechnique de Montreal. The authors are grateful to Dr. Haipeng Tang at National Research Council Canada for different critical insights on the manuscript. We also wish to thank Mr. H. M. Usama in the Department of Materials Science and Engineering at Massachusetts Institute of Technology (MIT) for useful discussions.

References

1. Palmstrm, C. J. *Annu. Rev. Mater. Sci.* **1995,** 25, 389-415.

2. Pezzagna, S.; Vézian, S.; Brault, J.; Massies, J. *Applied Physics Letters* **2008,** 92, (23), 233111.

3. Liu, Q. Z.; Lau, S. S.; Perkins, N. R.; Kuech, T. F. *Applied Physics Letters* **1996,** 69, (12), 1722-1724.

4. Missous, M.; Rhoderick, E. H.; Singer, K. E. *Journal of Applied Physics* **1986,** 59, (9), 3189-3195.

5. J.E. Oh.; P. K. Bhattacharya.; J. Singh, W. D. Passos.; R. Clarke, N. Mestres.;R. Merlin, K.H. Chang and R. Gibala. *Surface Science* **1990,** 228, 16-19.

6. Missous, S. J. P. a. M. *Journal of Crystal Growth* **1999,** 196, 1-12.

7. Krogstrup, P.; Ziino, N. L.; Chang, W.; Albrecht, S. M.; Madsen, M. H.; Johnson, E.; Nygard, J.; Marcus, C. M.; Jespersen, T. S. *Nat Mater* **2015,** 14, (4), 400-6.

8. Liu, Q. Z.; Shen, L.; Smith, K. V.; Tu, C. W.; Yu, E. T.; Lau, S. S.; Perkins, N. R.; Kuech, T. F. *Applied Physics Letters* **1997,** 70, (8), 990-992.

9. Uitsu Tanaka, T. M., Katsuhiro Akimoto. *Journal of Crystal growth* **1999,** 2001, 444-447.

10. Bermudez, V. M.; Kaplan, R.; Khan, M. A.; Kuznia, J. N. *Physical Review B* **1993,** 48, (4), 2436-2444.

11. Bermudez, V. M.; Jung, T. M.; Doverspike, K.; Wickenden, A. E. *Journal of Applied Physics* **1996,** 79, (1), 110-119.

12. Sadaf, S. M.; Ra, Y. H.; Szkopek, T.; Mi, Z. *Nano Lett* **2016,** 16, (2), 1076-80.

13. P.D. Browna, M. F., N. Bock, S. Marlafeka, T.S. Chengb, S.V. Novikov, C.S. Davis, R.P. Campion, C.T. Foxon. *Journal of Crystal Growth* **2000,** 234, (202), 384-390.

14. Meijers, R.; Calarco, R.; Kaluza, N.; Hardtdegen, H.; Ahe, M. v. d.; Bay, H. L.; Lüth, H.; Buchmeier, M.; Bürgler, D. E. *Journal of Crystal Growth* **2005,** 283, (3-4), 500-507.

15. Leonard, J. T.; Young, E. C.; Yonkee, B. P.; Cohen, D. A.; Margalith, T.; DenBaars, S. P.; Speck, J. S.; Nakamura, S. *Applied Physics Letters* **2015,** 107, (9), 091105.

16. Sadaf, S. M.; Ra, Y. H.; Nguyen, H. P.; Djavid, M.; Mi, Z. *Nano Lett* **2015,** 15, (10), 6696-701.

17. Zhao, S.; Connie, A. T.; Dastjerdi, M. H.; Kong, X. H.; Wang, Q.; Djavid, M.; Sadaf, S.; Liu, X. D.; Shih, I.; Guo, H.; Mi, Z. *Sci Rep* **2015,** 5, 8332.

18. Sarwar, A. T.; Carnevale, S. D.; Yang, F.; Kent, T. F.; Jamison, J. J.; McComb, D. W.; Myers, R. C. *Small* **2015,** 11, (40), 5402-8.

19. Kumaresan, V.; Largeau, L.; Madouri, A.; Glas, F.; Zhang, H.; Oehler, F.; Cavanna, A.; Babichev, A.; Travers, L.; Gogneau, N.; Tchernycheva, M.; Harmand, J. C. *Nano Lett* **2016,** 16, (8), 4895-902.

20. Zhao, S.; Sadaf, S. M.; Vanka, S.; Wang, Y.; Rashid, R.; Mi, Z. *Applied Physics Letters* **2016,** 109, (20), 201106.

21. Sadaf, S. M.; Zhao, S.; Wu, Y.; Ra, Y. H.; Liu, X.; Vanka, S.; Mi, Z. *Nano Lett* **2017**, 17 (2), 1212-1218.

22. Young, E. C.; Yonkee, B. P.; Wu, F.; Oh, S. H.; DenBaars, S. P.; Nakamura, S.; Speck, J. S. *Applied Physics Express* **2016,** 9, (2), 022102.

23. Zhang, Y.; Krishnamoorthy, S.; Johnson, J. M.; Akyol, F.; Allerman, A.; Moseley, M. W.; Armstrong, A.; Hwang, J.; Rajan, S. *Applied Physics Letters* **2015,** 106, (14), 141103.

24. Akyol, F.; Krishnamoorthy, S.; Zhang, Y.; Rajan, S. *Applied Physics Express* **2015,** 8, (8), 082103.

25. Akyol, F.; Krishnamoorthy, S.; Rajan, S. *Applied Physics Letters* **2013,** 103, (8), 081107.

26. Zhang, K.; Liang, H.; Liu, Y.; Shen, R.; Guo, W.; Wang, D.; Xia, X.; Tao, P.; Yang, C.; Luo, Y.; Du, G. *Sci Rep* **2014,** 4, 6322.

27. Chen, F.; Ji, X.; Zhang, Q. *CrystEngComm* **2015,** 17, (6), 1249-1257.

28. Kang, S.; Nandi, R.; Kim, H.; Jeong, K.-U.; Lee, C.-R. *Journal of Materials Chemistry C* **2018,** 6, (5), 1176-1186.

29. Limbach, F.; Caterino, R.; Gotschke, T.; Stoica, T.; Calarco, R.; Geelhaar, L.; Riechert, H. *AIP Advances* **2012,** 2, (1), 012157.

30. Miceli, G.; Pasquarello, A. *Physical Review B* **2016,** 93, (16).

31. Okumura, H.; Martin, D.; Grandjean, N. *Applied Physics Letters* **2016,** 109, (25), 252101.

32. Mahaveer Sathaiya, D.; Karmalkar, S. *Journal of Applied Physics* **2006,** 99, (9), 093701.

33. Okumura, H.; Martin, D.; Malinverni, M.; Grandjean, N. *Applied Physics Letters* **2016,** 108, (7), 072102.

34. J. D. Hwang, Y. K. F., K. H. Chen, and D. N. Yaung *IEEE Electron Device Letters* **1995,** 16, (5), 193-195.

35. Ra, Y. H.; Wang, R.; Woo, S. Y.; Djavid, M.; Sadaf, S. M.; Lee, J.; Botton, G. A.; Mi, Z. *Nano Lett* **2016,** 16, (7), 4608-15.

FIGURE CAPTIONS

Figure 1 (a) Schematic illustration of different epitaxial Al/Al(Ga)N nanostructures grown on Si substrates, including nanostructure A (Al~1.6 nm), nanostructure B (Al~5 nm) and nanostructure C (Al~15 nm). (b) An SEM image of nanostructure A taken with a 45° angle. The scale bar denotes 1 μm. (c) High-resolution transmission electron microscopy (HR-TEM) image of nanostructure B. The image shows the interface between Al/*n*-GaN and Al/*p*-Al(Ga)N. The image also shows the interplanar spacings of Al (111), *n*-GaN (0002) and *p*-AlGaN (0002) planes.

Figure 2 (a) STEM image of a full nanostructure C (thick Al layer, nanostructure C) (b) EDXS point analysis of the Al layer (point B in b) and *p*-AlGaN region (point C in b), *n*-GaN region (point A in b) and Al layer in sidewall region (point D in b) and (c) EDXS comparative point analysis of Al and Ga in different regions shown in b.

Figure 3 (a) STEM image of a nanostructure C (thick Al layer) and (b) different EDXS line scan analysis along the nanowire length (line A) and lateral dimension (line B and C). The line scans show the presence of AlGaN shell.

Figure 4 Symmetric θ/2θ X-ray diffraction analysis of *n*-GaN/Al/*p*-Al(Ga)N nanostructures in Bragg reflection. The diffraction peaks confirm the epitaxy between Al (111) and GaN (0002).

Figure 5 a) I-V characteristics comparison of n^{++}-GaN/Al/p^{++}-$Al_{0.15}Ga_{0.85}N$ backward diode structure (Diode A) and n^{++}-GaN/Al/p^{+}-$Al_{0.50}Ga_{0.50}N$ (Diode B), the inset shows I-V characteristics comparison of n^{+}- $Al_{0.50}Ga_{0.50}N$ /Al/p^{+}-$Al_{0.50}Ga_{0.50}N$ backward diode structure (Diode C) and n^{+}-AlN/Al/p^{+}-AlN backward structure (Diode D) (b) Schematic energy band diagram of n^{++}-GaN/Al/p^{++}-$Al_{0.15}Ga_{0.85}N$ backward diode structures (Diode A) and (c) n^{++}-

GaN/Al/p^{++}-$Al_{0.50}Ga_{0.50}N$ backward structure (Diode B). (d) Temperature dependent I-V characteristics comparison of n^{++}-GaN/Al/p^{++}-$Al_{0.15}Ga_{0.85}N$ backward diode structure (Diode A).

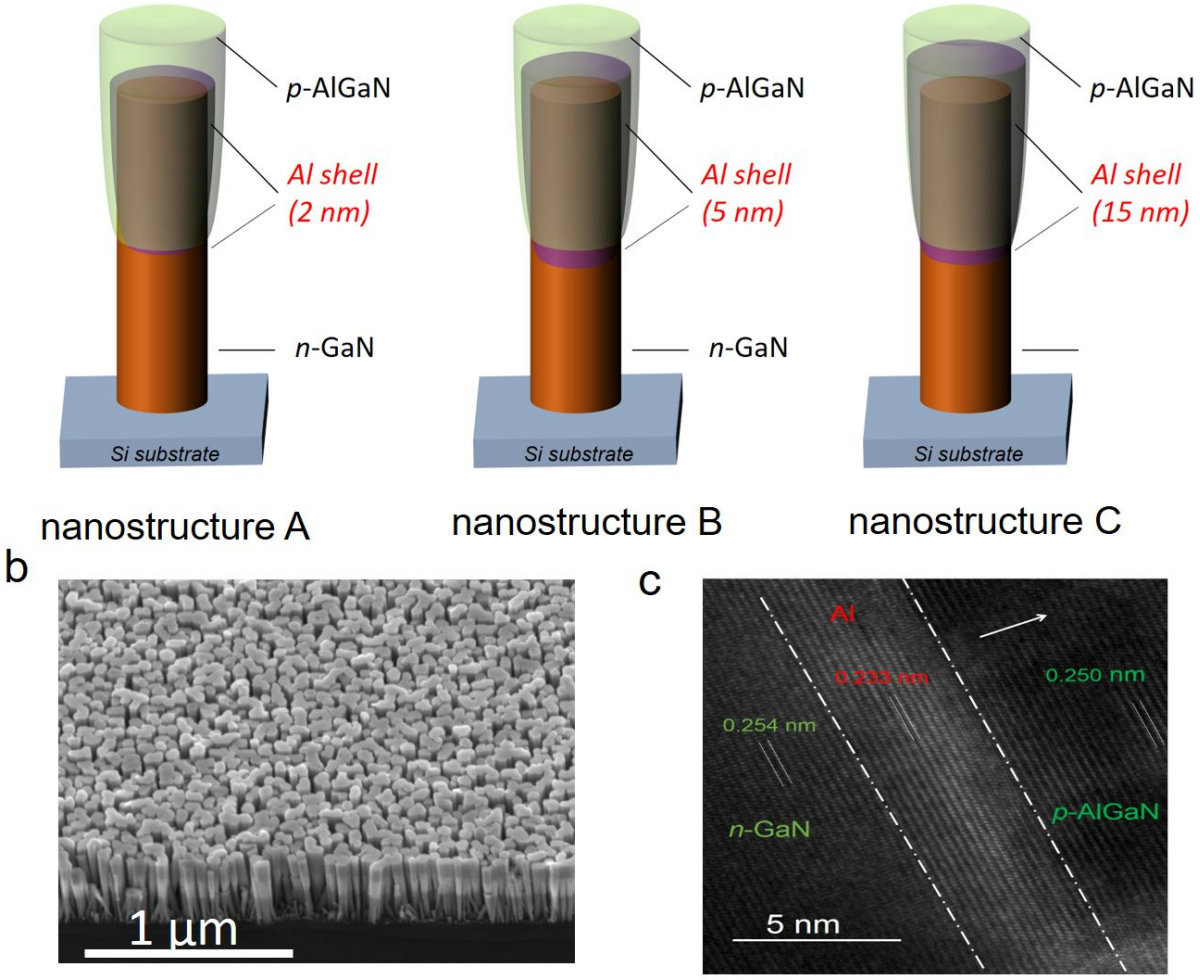
p-AlGaN
Al shell
(2 nm)
n-GaN
Si substrate
nanostructure A
p-AlGaN
Al shell
(5 nm)
n-GaN
Si substrate
nanostructure B
p-AlGaN
Al shell
(15 nm)
Si substrate
nanostructure C
b
1 μm
c
Al
0.233 nm
0.250 nm
0.254 nm
n-GaN
p-AlGaN
5 nm

Figure 1

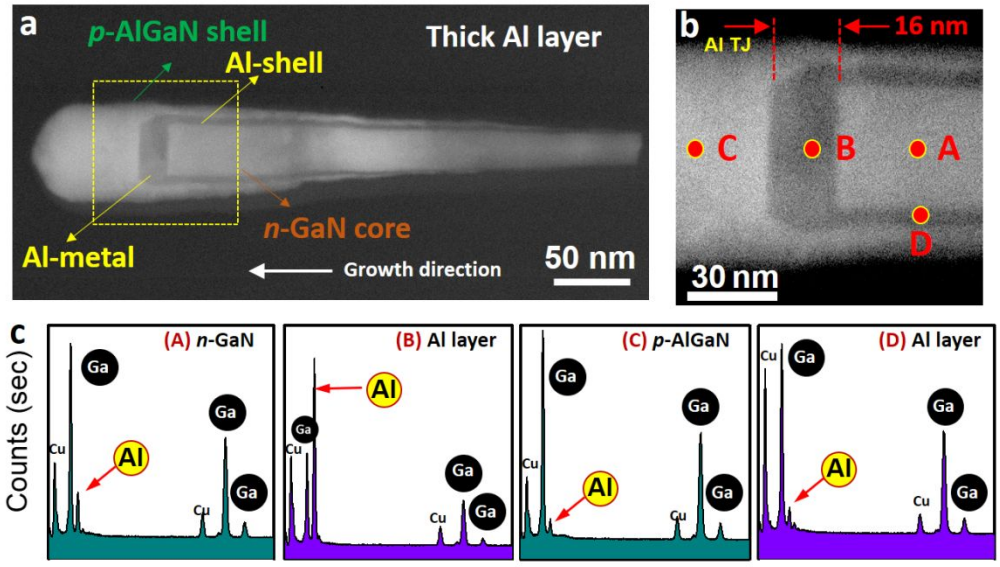
a
p-AlGaN shell
Al-shell
Thick Al layer
n-GaN core
Al-metal
Growth direction
50 nm
b
Al TJ
16 nm
C
B
A
D
30 nm
c
Counts (sec)
(A) n-GaN
(B) Al layer
(C) p-AlGaN
(D) Al layer
Ga
Al
Cu

Figure 2

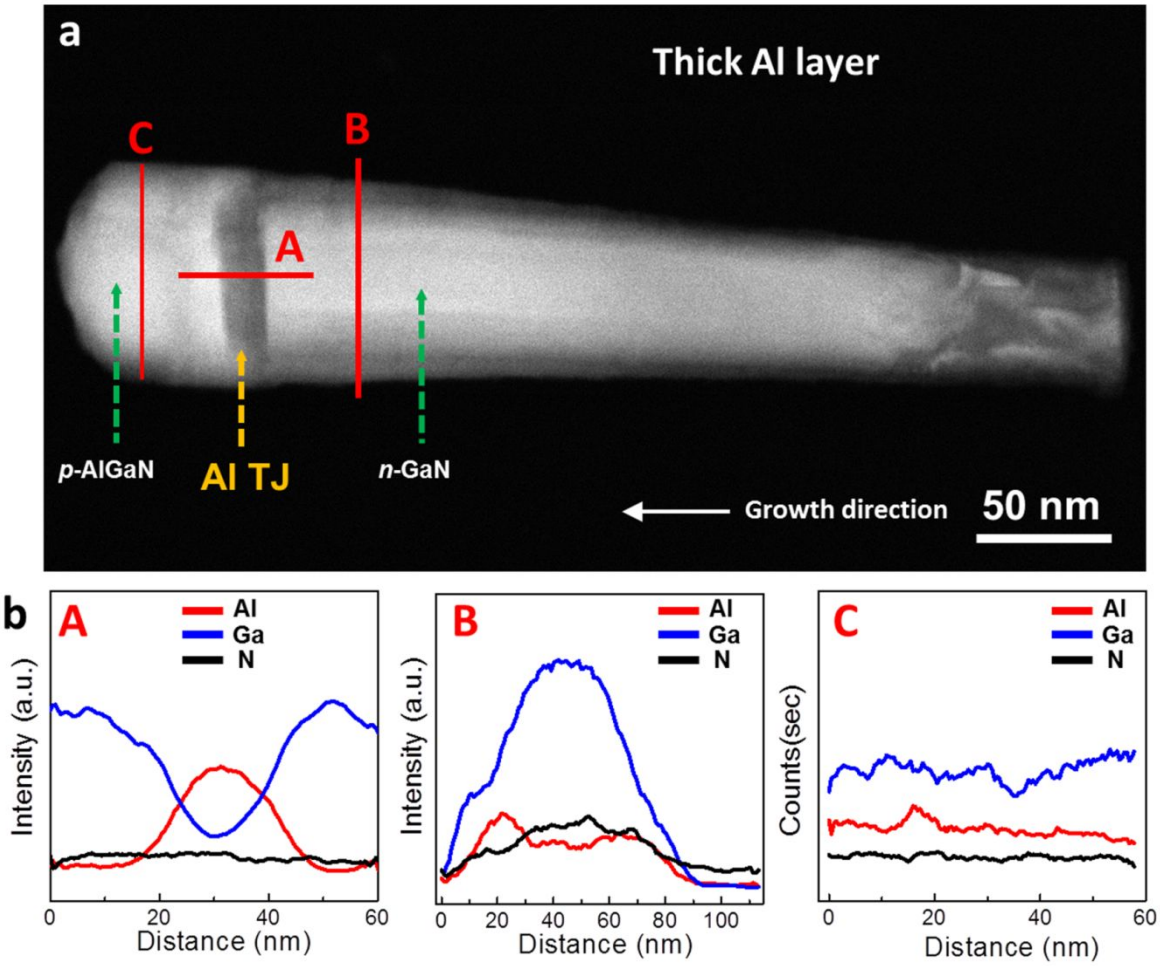
a
Thick Al layer
C
B
A
p-AlGaN
Al TJ
n-GaN
Growth direction
50 nm
b
A
B
C
Al
Ga
N
Intensity (a.u.)
Counts(sec)
Distance (nm)
0
20
40
60
80
100

Figure 3

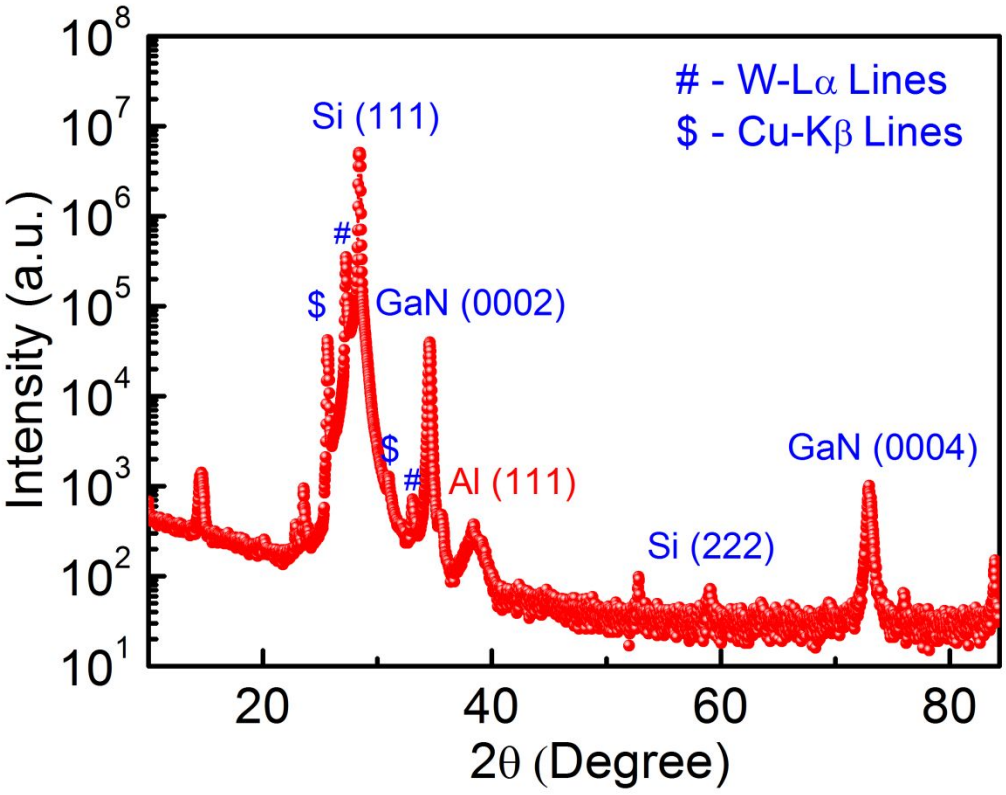
Intensity (a.u.)
2θ (Degree)
- W-Lα Lines
$ - Cu-Kβ Lines
Si (111)
#
$
GaN (0002)
$
#
Al (111)
Si (222)
GaN (0004)

Figure 4

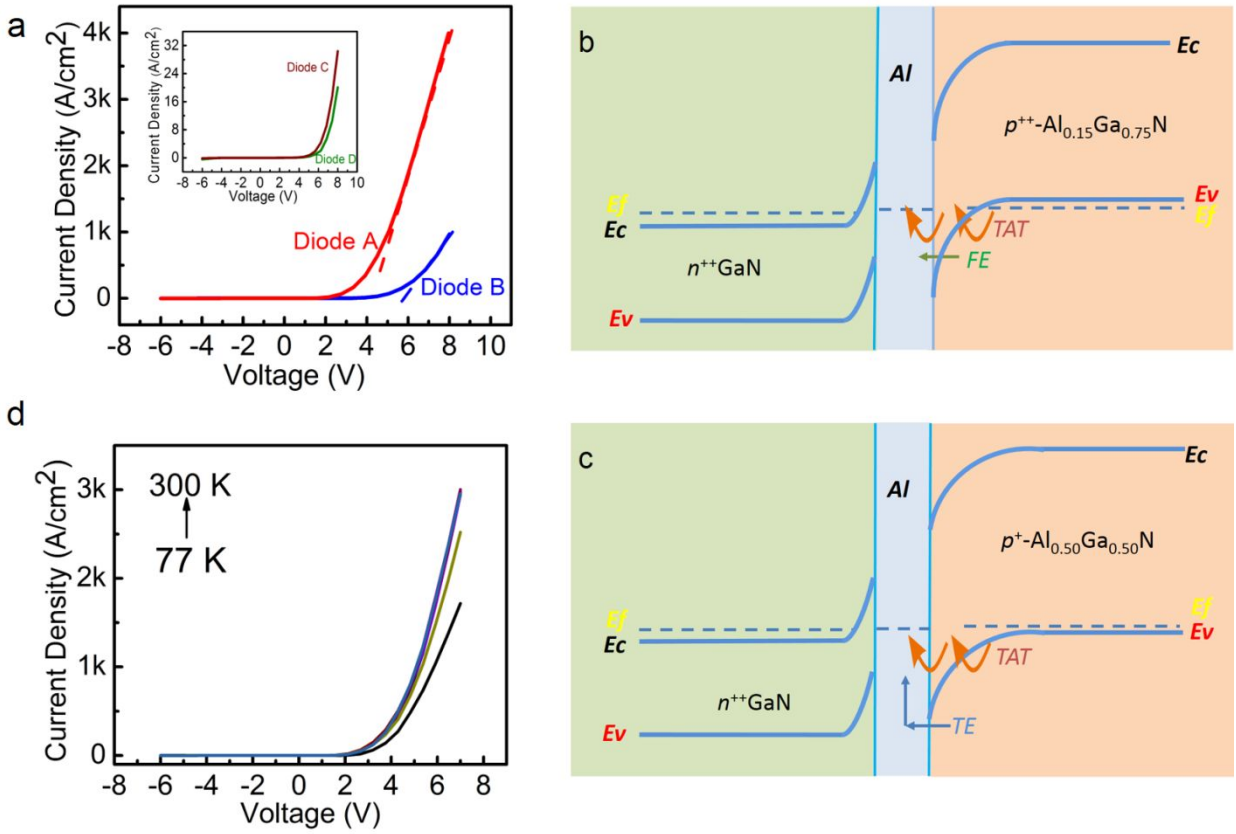
a
Current Density (A/cm2)
Voltage (V)
Diode A
Diode B
Diode C
Diode D
b
Al
Ec
p++-Al0.15Ga0.75N
Ef
Ev
n++GaN
TAT
FE
c
p+-Al0.50Ga0.50N
TE
d
300 K
77 K

Figure 5